

Shell-model studies of the astrophysical rp -process reactions $^{34}\text{S}(p, \gamma)^{35}\text{Cl}$ and $^{34g,m}\text{Cl}(p, \gamma)^{35}\text{Ar}$

W. A. Richter^{1,2,*} B. A. Brown^{3,9,†} R. Longland⁴ C. Wrede^{3,9} P. Denissenkov^{5,‡}
C. Fry³ F. Herwig^{5,9,‡} D. Kurtulgil^{6,‡} M. Pignatari^{7,8,9,‡} and R. Reifarth^{6,‡}

¹University of Stellenbosch, Stellenbosch 7600, South Africa

²iThemba LABS, Somerset West 7130, South Africa

³Department of Physics and Astronomy and National Superconducting Cyclotron Laboratory,
Michigan State University, East Lansing, Michigan 48824-1321, USA

⁴Department of Physics, North Carolina State University, Raleigh NC 27695, USA
and Triangle Universities Nuclear Laboratory, Duke University, Durham NC 27710, USA

⁵Department of Physics and Astronomy, University of Victoria, Victoria, British Columbia V8W 2Y2, Canada

⁶Goethe University Frankfurt, Max-von-Laue-Strasse 1, Frankfurt am Main 60438, Germany

⁷E.A. Milne Center for Astrophysics, Department of Physics and Mathematics, University of Hull, Hull HU6 7RX, United Kingdom

⁸Konkoly Observatory, Research Center for Astronomy and Earth Sciences, Hungarian Academy of Sciences,
Konkoly Thege Miklos ut 15-17, H-1121 Budapest, Hungary

⁹Joint Institute for Nuclear Astrophysics—Center for the Evolution of the Elements, Michigan State University,
East Lansing, Michigan 48824, USA



(Received 30 December 2019; accepted 28 May 2020; published 4 August 2020)

Background: Dust grains condensed in the outflows of presolar classical novae should have been present in the protosolar nebula. Candidates for such presolar nova grains have been found in primitive meteorites and can in principle be identified by their isotopic ratios, but the ratios predicted by state-of-the-art one-dimensional hydrodynamic models are uncertain due to nuclear-physics uncertainties.

Purpose: To theoretically calculate the thermonuclear rates and uncertainties of the $^{34}\text{S}(p, \gamma)^{35}\text{Cl}$ and $^{34g,m}\text{Cl}(p, \gamma)^{35}\text{Ar}$ reactions and investigate their impacts on the predicted $^{34}\text{S}/^{32}\text{S}$ isotopic ratio for presolar nova grains.

Method: A shell-model approach in a $(0 + 1) \hbar\omega$ model space was used to calculate the properties of resonances in the $^{34}\text{S}(p, \gamma)^{35}\text{Cl}$ and $^{34g,m}\text{Cl}(p, \gamma)^{35}\text{Ar}$ reactions and their thermonuclear rates. Uncertainties were estimated using a Monte Carlo method. The implications of these rates and their uncertainties on sulfur isotopic nova yields were investigated using a postprocessing nucleosynthesis code. The rates for transitions from the ground state of ^{34}Cl as well as from the isomeric first excited state of ^{34}Cl were explicitly calculated.

Results: At energies in the resonance region near the proton-emission threshold, many negative-parity states appear. Energies, spectroscopic factors, and proton-decay widths are reported. The resulting thermonuclear rates are compared with previous determinations.

Conclusions: The shell-model calculations alone are sufficient to constrain the variation of the $^{34}\text{S}/^{32}\text{S}$ ratios to within about 30%. Uncertainties associated with other reactions must also be considered, but in general we find that the $^{34}\text{S}/^{32}\text{S}$ ratios are not a robust diagnostic to clearly identify presolar grains made from nova ejecta.

DOI: [10.1103/PhysRevC.102.025801](https://doi.org/10.1103/PhysRevC.102.025801)

I. INTRODUCTION

A classical nova is a thermonuclear explosion on the surface of a white dwarf star accreting hydrogen-rich gas from a companion star in a binary system. In cooling nova outflows, material that has undergone nucleosynthesis can condense to form dust grains. Such grains should have been present in the protosolar nebula and can be searched for in primitive meteorites and, in principle, identified by their isotopic ratios. Indeed, several candidate presolar nova grains have been recovered but their identifications are often ambiguous due to

uncertainties associated with the thermonuclear reaction rates in novae.

For example, the $^{34}\text{S}/^{32}\text{S}$ ratio has the potential to aid in presolar novae grain classification, but the nuclear reaction rate uncertainties are too large for it to be an unambiguous tool [1]. ^{34}S can be destroyed in novae through the $^{34}\text{S}(p, \gamma)^{35}\text{Cl}$ reaction or bypassed by the $^{34}\text{Cl}(p, \gamma)^{35}\text{Ar}$ reaction if the rate is fast enough to dominate the β -decay rate $^{34}\text{Cl} \rightarrow ^{34}\text{S}$ ($T_{1/2} = 1.53$ s for the ground state). The thermonuclear rates of these reactions are unknown at nova temperatures due to a lack of experimental nuclear physics data for the resonances up to about 800 keV above the ^{35}Ar proton separation energy [2]. Moreover, some nova models treat the $^{33}\text{S}(p, \gamma)^{34}\text{Cl}$ and $^{34}\text{Cl}(p, \gamma)^{35}\text{Ar}$ rates as total rates, without separately considering the ground state ^{34g}Cl and the isomeric first excited state ^{34m}Cl ($E_x = 0.146$ keV, $T_{1/2} = 2.5$ min). However,

*richter.werner@gmail.com

†brown@nscl.msu.edu

‡NuGrid Collaboration, <https://nugrid.github.io>

similar to the case of ^{26}Al , the ^{34}Cl ground state and its long-lived isomer are not necessarily in thermal equilibrium at nova temperatures and it is therefore necessary to calculate the reaction rates on both initial states, in order to represent their influence accurately in a nucleosynthesis calculation [3–5], and in some cases capture on an excited state can dominate a thermonuclear reaction rate even when it is in thermal equilibrium with the ground state [6]. Therefore, it is important to constrain not only the $^{34g}\text{Cl}(p, \gamma)^{35}\text{Ar}$ reaction rate, but also the $^{34m}\text{Cl}(p, \gamma)^{35}\text{Ar}$ rate.

In a recent experiment [7], the $^{34}\text{S}(^3\text{He}, d)^{35}\text{Cl}$ reaction was studied and proton-transfer spectroscopic factors were measured for 21 states in an excitation energy region of 1 MeV above the $^{34}\text{S}(p, \gamma)$ threshold energy ($S_p = 6.371$ MeV). The experimental cross sections are proportional to $\text{C}^2\text{S}^+ = [(2J_f + 1)/(2J_i + 1)] \text{C}^2\text{S}$ ($J_i = 0$ in this case), the same quantity that enters the reaction rate. It is not necessary to determine the J_f values of the resonances explicitly. These results were considered in Ref. [8] to obtain the $^{34}\text{S}(p, \gamma)^{35}\text{Cl}$ reaction rate. We will compare our calculations with these results.

In a study by Fry *et al.* [2], 17 ^{35}Ar levels have been detected in the energy region $E_x = 5.9$ –6.7 MeV and their excitation energies have been determined, but not spins, parities, widths, or branching ratios. Because of the paucity of such information, it is not yet possible to derive meaningful experimental $^{34g,m}\text{Cl}(p, \gamma)^{35}\text{Ar}$ reaction rates.

Estimates based on shell-model calculations are complicated by high level density and the presence of negative-parity states in the resonance region near the proton-emission threshold. To address this problem, we present calculations of $^{35}\text{Cl} + p$ and $^{35}\text{Ar} + p$ resonances in a $(0 + 1) \hbar\omega$ basis with the code NUSHELLX [9] to provide energies, spectroscopic factors, and proton-decay widths. Such calculations were carried out recently for the $^{30}\text{P}(p, \gamma)^{31}\text{S}$ reaction [10].

We use the shell-model results to calculate the thermonuclear rates for radiative proton capture reactions on the ground states of ^{34}S and ^{34}Cl , and on the isomeric first-excited state of ^{34}Cl . Uncertainties for the total calculated reaction rates have been included based on Monte Carlo techniques [11]. The implications of these rates on the predicted $^{34}\text{S}/^{32}\text{S}$ ratio in presolar nova grains have been investigated using a postprocessing nova nucleosynthesis code.

The results given in this paper supersede those given in the preliminary conference series publication [12].

II. THE SHELL-MODEL CALCULATIONS

For positive-parity states, we use the $(1s_{1/2}, 0d_{5/2}, 0d_{3/2})$ (*sd*) model space with the universal *sd*-shell version B (USDB) Hamiltonian [13]. For negative-parity states, the model space is extended to include $1\hbar\omega$ excitations. This involves one nucleon excited from the $(0p_{3/2}, 0p_{1/2})$ (*p*) shell to the *sd* shell, or one nucleon excited from the *sd* shell to the $(1p_{1/2}, 1p_{3/2}, 0f_{7/2}, 0f_{5/2})$ (*pf*) shell. The spurious states for these $1\hbar\omega$ negative-parity states were removed using the Gloeckner-Lawson method [14]. For $1\hbar\omega$, we start with the Warburton-Brown potential-model (WBP) Hamiltonian from [15]. The *sd* part of the WBP was based on the older universal

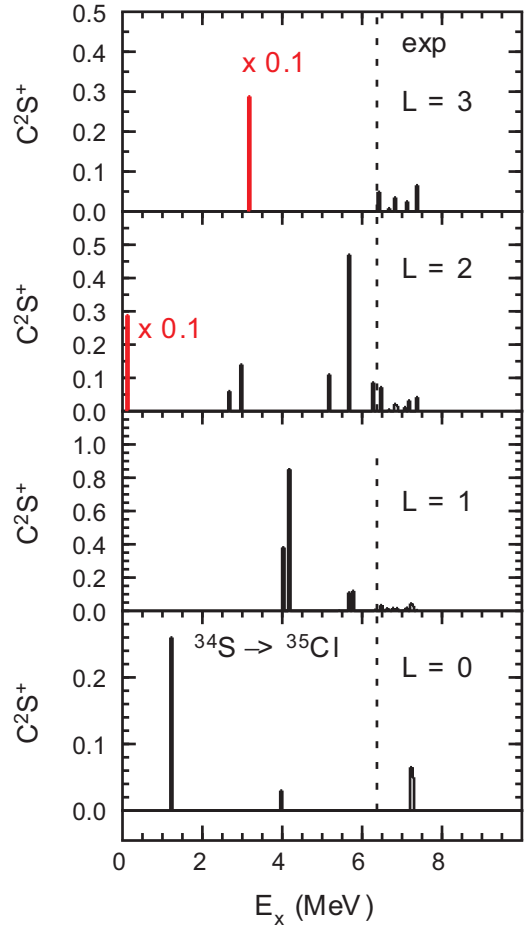


FIG. 1. Experimental spectroscopic factors, $\text{C}^2\text{S}^+ = (2J_f + 1) \text{C}^2\text{S}$, for single-proton transfer on the target ^{34}S . The results below 5.8 MeV are from Ref. [19], and the results from 6.2 to 7.4 MeV are from Ref. [7]. The dotted line shows the value of the proton separation energy.

sd-shell (USD) Hamiltonian [16]. We have replaced that part with the USDB Hamiltonian. The wave functions for $1\hbar\omega$ negative-parity states in the nuclei we consider are dominated by the *sd* to *pf* excitations. That part of the WBP Hamiltonian is based on the WBMB Hamiltonian obtained for the *sd*-*pf* model space in Ref. [17]. For our purpose, the single-particle energies for $1p_{1/2}$, $1p_{3/2}$, and $0f_{7/2}$ were adjusted to reproduce the energies of the strongest states observed in the one-nucleon transfer reactions from ^{34}S to ^{35}S and ^{35}Cl . The spin-orbit splitting for $0f_{7/2}$ – $0f_{5/2}$ was set to 6 MeV.

The effective operators for *M1* and *E2* γ decay are taken from Ref. [18]. We use the free-nucleon operator for *E1* γ decay. But we note that all of the reaction rates considered here are dominated by the proton-decay width, and thus the uncertainty in the rates coming from the γ decay rates is negligible.

For the (p, γ) reactions, the most important aspects of the calculation are the energies and the one-nucleon spectroscopic factors. The best data for this comparison is the one-nucleon transfer data from ^{34}S to ^{35}Cl . The experimental spectroscopic factors, $\text{C}^2\text{S}^+ = (2J_f + 1) \text{C}^2\text{S}$, are shown in Fig. 1, and the theoretical results are shown in Fig. 2. The results for 16 states

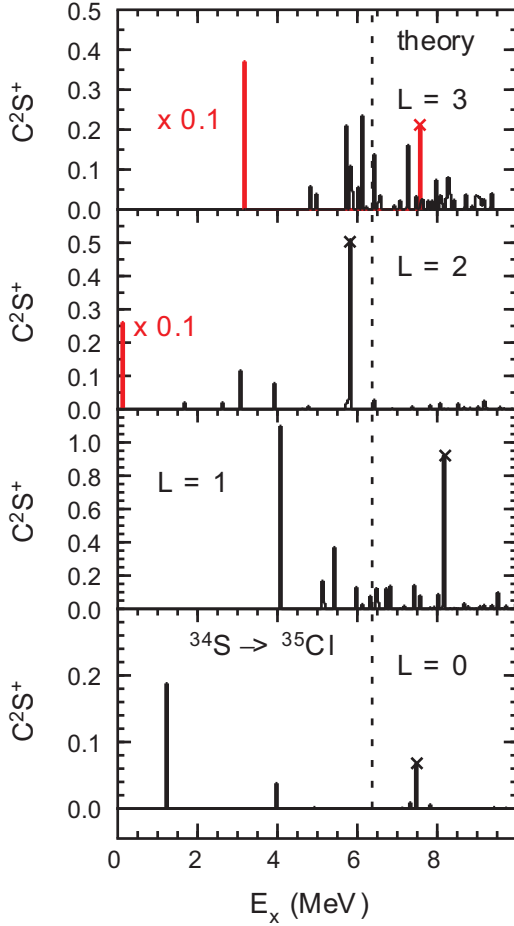


FIG. 2. Theoretical spectroscopic factors, $C^2S^+ = (2J_f + 1) C^2S$, for single-proton transfer on the target ^{34}S . The states with $T = 3/2$ are indicated by a cross on top. The dotted line shows the value of the proton separation energy.

below 5.8 MeV are from Ref. [19], and the results for 21 states from 6.2 to 7.4 MeV are from Ref. [7]. The spectroscopic factors have not been measured between 5.8 and 6.3 MeV. Many of the states observed [7] are assigned $L = (0, 1)$. Our calculations indicate that there are many more states with $L = 1$ in this energy region compared to those with $L = 0$. For the purpose of comparison, we show the spectroscopic factors for these as $L = 1$ in Fig. 1.

The results for positive-parity states based on the USDB Hamiltonian are in good agreement with experiment. The relatively strong $L = 2$ state near 5.7 MeV is the $T = 3/2$ isobaric analog of the ^{35}S $3/2^+$ ground state. The relatively strong $L = 0$ state near 7.2 MeV is the $T = 3/2$ isobaric analog of the ^{35}S $1/2^+$ first excited state.

The results for negative-parity states are in reasonable agreement with experiment. The results from Ref. [7] do not have unique L values or J_f assignments, and we are not able to make a state-by-state comparison. Between 6.2 and 7.4 MeV, 21 states are observed experimentally [7] compared to 40 states with $J_f^\pi = 1/2^+, 3/2^+, 5/2^+, 1/2^-, 3/2^-, 5/2^-$, and $7/2^-$ calculated. Many of these states may have not been observed due to their very small spectroscopic factors. The strong $L = 3$ states near 5.9 MeV are in the energy window of

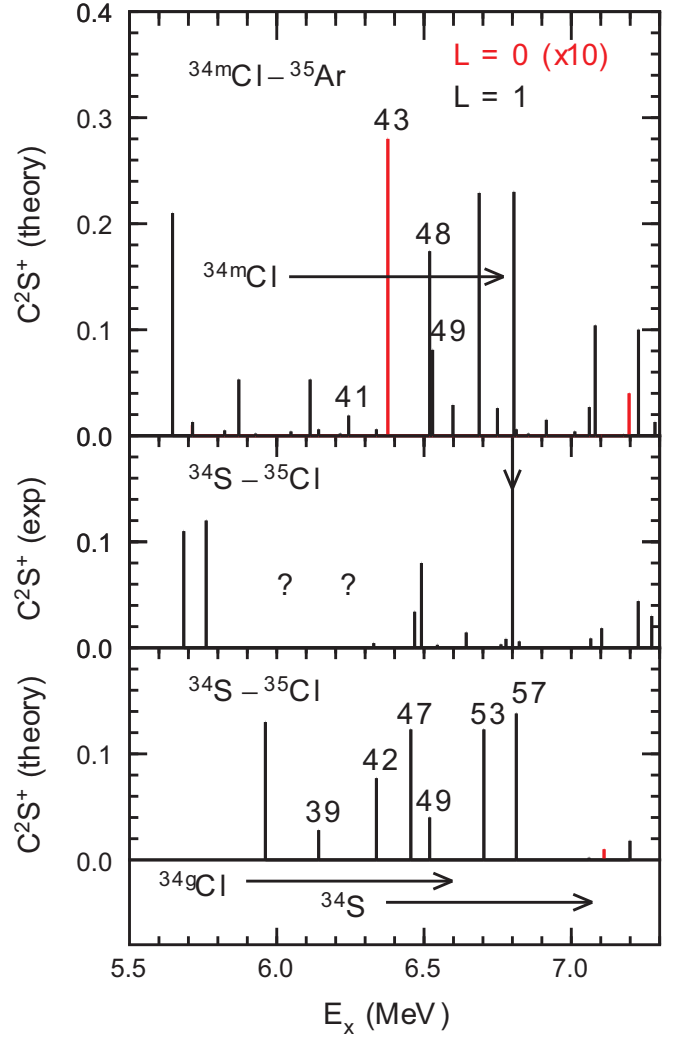


FIG. 3. Spectroscopic factors, C^2S^+ , for $L = 0, 1$ in the excitation energy region of importance for the reactions rates. For a given spectroscopic factor, $L = 0$ is about a factor of 10 stronger than $L = 1$ in the reaction rate due to the smaller centrifugal barrier. For this reason, the values for $L = 0$ have been multiplied by 10 to show their relative importance to $L = 1$. The bottom panel shows the theoretical values for ^{34}S to ^{35}Cl . The peaks are labeled by their order in the excitation energy spectrum. The middle panel shows the experiment values from Ref. [19] for $E_x < 5.8$ MeV and from Refs. [7] and [8] for $E_x > 6.3$ MeV. Experimental results are not known for the region between 5.8 and 6.3 MeV. The line at 6.8 MeV labeled by a down arrow is given in Ref. [8] by $C^2S^+ < 4$. The arrows at the bottom show the range of excitation energy important for the $^{34}\text{S}(p, \gamma)^{35}\text{Cl}$ reaction starting at $S_p = 6.371$ MeV, and the $^{34g}\text{Cl}(p, \gamma)^{35}\text{Ar}$ starting at $S_p = 5.896$ MeV in the mirror nucleus ^{35}Ar . The upper panel shows the spectroscopic factors for $^{34m}\text{Cl}(3^+)(p, \gamma)^{35}\text{Ar}$. The arrow starting at $S_p = 6.042$ MeV shows the range of excitation energy of importance for that reaction. These spectroscopic factors lead to a reaction rate for $^{34m}\text{Cl}(3^+)(p, \gamma)^{35}\text{Ar}$ that is about a factor of 4 larger than that for $^{34g}\text{Cl}(0^+)(p, \gamma)^{35}\text{Ar}$ in the region around $T_9 = 0.2$ GK.

5.8 to 6.3 MeV not covered by experiment. The strong $L = 3$ state near 7.3 MeV is the $T = 3/2$ isobaric analog of the ^{35}S $7/2^-$ third excited state. The relatively strong $L = 1$ state

TABLE I. Properties of the resonance states for $^{34}\text{S}(p, \gamma)^{35}\text{Cl}$ from 5.8 to 7.2 MeV. $J_i^\pi = 0^+$. $Q = 6.371$ MeV. n is the number of the level in the spectrum. k is the number of the level for a given J^π value. $\text{C}^2\text{S}^+ = [(2J_f + 1)/(2J_i + 1)] \text{C}^2\text{S}$.

n	J^π	k	$E_x(\text{th})$ (MeV)	E_{res} (MeV)	C^2S^+ $\ell = 0(1)$	Γ_γ (eV)	Γ_p (eV)	$\omega\gamma$ (eV)
2	$1/2^+$	1	1.226		1.9×10^{-1}	1.8×10^{-3}		
9	$1/2^+$	2	3.981		3.8×10^{-2}	2.2×10^{-2}		
10	$3/2^-$	1	4.079		1.1	2.7×10^{-2}		
17	$1/2^+$	3	4.930		2.3×10^{-3}	1.3×10^{-1}		
20	$3/2^-$	2	5.119		1.7×10^{-1}	8.0×10^{-2}		
21	$1/2^-$	1	5.182		3.5×10^{-2}	1.3×10^{-2}		
23	$3/2^-$	3	5.429		3.7×10^{-1}	2.5×10^{-2}		
35	$1/2^-$	2	5.961		1.3×10^{-1}	2.6×10^{-1}		
39	$3/2^-$	4	6.142		2.8×10^{-2}	5.3×10^{-2}		
42	$3/2^-$	5	6.338		7.7×10^{-2}	2.8×10^{-1}		
47	$1/2^-$	3	6.455	0.084	1.2×10^{-1}	1.7×10^{-1}	3.3×10^{-15}	3.3×10^{-15}
49	$3/2^-$	6	6.519	0.148	4.0×10^{-2}	2.1×10^{-1}	3.1×10^{-10}	6.3×10^{-10}
53	$1/2^-$	4	6.703	0.332	1.2×10^{-1}	2.1×10^{-1}	1.3×10^{-3}	1.3×10^{-3}
57	$3/2^-$	7	6.813	0.442	1.4×10^{-1}	1.9×10^{-1}	2.6×10^{-2}	4.6×10^{-2}
63	$3/2^-$	8	7.060	0.689	1.9×10^{-3}	1.3×10^{-1}	3.6×10^{-2}	5.7×10^{-2}
67	$1/2^+$	4	7.112	0.741	1.1×10^{-3}	9.3×10^{-1}	2.3×10^{-1}	1.9×10^{-1}
68	$3/2^-$	9	7.177	0.806	4.0×10^{-4}	2.6×10^{-1}	2.9×10^{-2}	5.3×10^{-2}
70	$1/2^-$	5	7.198	0.827	1.8×10^{-2}	1.9×10^{-1}	3.2	1.8×10^{-1}
72	$1/2^+$	5	7.305	0.934	9.0×10^{-3}	2.0	1.2×10^1	1.7
78	$1/2^-$	6	7.415	1.044	1.3×10^{-1}	2.3×10^{-1}	1.4×10^2	2.3×10^{-1}

near 8.2 MeV is the $T = 3/2$ isobaric analog of the ^{35}S $3/2^-$ fourth excited state.

The strongest $L = 1$ state at 4.1 MeV is $3/2^-$. In the experiment, this strength gets split over two nearby $3/2^-$ states separated by 118 keV. The second $3/2^-$ state cannot be reproduced by the calculation. This is a potential problem with the calculation, but it may be $3\hbar\omega$ related to a ^{32}S plus $(fp)^3$ cluster-type structure. This could explain the near degeneracy of two states with the same J^π . These $3\hbar\omega$ configurations would not directly contribute to the one-nucleon spectroscopic strengths, but they would introduce more states in the spectrum and cause the spectroscopic strength to be split over nearby states as is the case with these $3/2^-$ states.

We consider the reactions $^{34}\text{S}(0^+)(p, \gamma)^{35}\text{Cl}$ and $^{34g}\text{Cl}(0^+)(p, \gamma)^{35}\text{Ar}$. The initial states are isobaric analogs, and the final nuclei are mirrors of each other. The nuclear structure input is the same except that the spectroscopic factors to ^{35}Ar are reduced a factor of 2 compared to those to ^{35}Cl due to the difference in the C^2 factor. The energy shifts between the states in these mirror nuclei depend on the state and are on the order of a hundred keV or less.

We also consider the reaction rate for $^{34m}\text{Cl}(3^+)(p, \gamma)^{35}\text{Cl}$ from the isomeric state at 146 keV in ^{34}Cl . All three of these reactions depend on the properties of states in the region of 6–7 MeV in ^{35}Cl and ^{35}Ar .

In the $^{36}\text{Ar}(d, t)^{35}\text{Ar}$ reaction [2], 22 levels were observed between 5.9 and 6.7 MeV in ^{35}Ar . Our shell-model results have 19 levels in this region of excitation energy. In Refs. [7] and [8], 15 levels with $J < 5/2$ are observed between 6.3 and 7.0 MeV in ^{35}Cl . Our shell-model results have 14 levels with $J < 5/2$ in this region of excitation energy. Given the

high level density, this is good agreement between theory and experiment.

III. RESULTS FOR THE REACTION RATES

We follow the standard procedures used to obtain reaction rates [11]. The shell-model calculations provide the spectroscopic factors and γ decay widths, Γ_γ . The proton decay width is obtained from $\Gamma_p = \text{C}^2\text{S}\Gamma_{sp}$, where Γ_{sp} is the single-particle proton decay based on the proton scattering from a Woods-Saxon potential [20]. These are then combined to obtain the $\omega\gamma$ and the reaction rates.

The contributions from $L = 0, 1$ are about an order of magnitude larger than those with $L = 2, 3$ due to the larger centrifugal barriers for the high L . The spectroscopic factors for $L = 0, 1$ in the excitation energy region of interest for our reaction rates are shown in Fig. 3. The details for the theoretical input to the reaction rates for $L = 0, 1$ are given in Tables I, II, and III. The reaction rates are shown in Figs. 4, 5, and 6. The bottom parts of these figures show the percentage contribution from each final state. The most important states are labeled by the state numbers shown in Fig. 3 and the tables.

We obtained uncertainties for the reaction rates based on Monte Carlo techniques [11]. The results for the quartiles of the cumulative reaction rate distribution for $^{34}\text{S}(p, \gamma)^{35}\text{Cl}$ are shown in Fig. 4. We assume 200-keV uncertainty for the resonance energy, and factor of 2 uncertainties for the γ -decay and proton-decay widths. The error in the rate from the γ decay width is negligible since, as shown in the tables, the

TABLE II. Properties of the resonance states for $^{34}\text{gCl}(p, \gamma)^{35}\text{Ar}$ from 5.8 to 6.8 MeV. $J_i^\pi = 0^+$. $Q = 5.896$ MeV. n is the number of the level in the spectrum. k is the number of the level for a given J^π value. $\text{C}^2\text{S}^+ = [(2J_f + 1)/(2J_i + 1)] \text{C}^2\text{S}$.

n	J^π	k	$E_x(\text{th})$ (MeV)	E_{res} (MeV)	C^2S^+ $\ell = 0(1)$	Γ_γ (eV)	Γ_p (eV)	$\omega\gamma$ (eV)
2	$1/2^+$	1	1.226		9.4×10^{-2}	1.0×10^{-3}		
9	$1/2^+$	2	3.981		1.9×10^{-2}	2.5×10^{-2}		
10	$3/2^-$	1	4.079		5.5×10^{-1}	2.7×10^{-2}		
17	$1/2^+$	3	4.930		1.1×10^{-3}	1.1×10^{-1}		
20	$3/2^-$	2	5.119		8.4×10^{-2}	7.9×10^{-2}		
21	$1/2^-$	1	5.182		1.8×10^{-2}	1.3×10^{-2}		
23	$3/2^-$	3	5.429		1.8×10^{-1}	2.5×10^{-2}		
35	$1/2^-$	2	5.961	0.065	6.5×10^{-2}	2.6×10^{-1}	3.6×10^{-20}	3.6×10^{-20}
39	$3/2^-$	4	6.142	0.246	1.4×10^{-2}	4.9×10^{-2}	1.9×10^{-7}	3.8×10^{-7}
42	$3/2^-$	5	6.338	0.442	3.9×10^{-2}	2.8×10^{-1}	2.4×10^{-3}	4.9×10^{-3}
47	$1/2^-$	3	6.455	0.559	6.2×10^{-2}	1.7×10^{-1}	1.2×10^{-1}	7.0×10^{-2}
49	$3/2^-$	6	6.519	0.623	2.0×10^{-2}	2.1×10^{-1}	6.2×10^{-2}	9.5×10^{-2}
53	$1/2^-$	4	6.703	0.807	6.2×10^{-2}	2.0×10^{-1}	4.5	1.9×10^{-1}
57	$3/2^-$	7	6.813	0.917	6.9×10^{-2}	1.9×10^{-1}	7.6	3.7×10^{-1}
63	$3/2^-$	8	7.061	1.165	9.7×10^{-4}	1.3×10^{-1}	6.8×10^{-1}	2.2×10^{-1}

proton-decay width is much smaller than the γ decay for those states in the excitation energy region that contribute to the rate.

In Fig. 5, our results for $^{34}\text{S}(p, \gamma)^{35}\text{Cl}$ are compared with the rate [8] based on experimental data from Ref. [7]. The Hauser-Feshbach rate from Ref. [21] is also shown. All of these are in relatively good agreement. This comparison with experiment indicates that our assumed uncertainties are reasonable.

Results for the $L = 0, 1$ spectroscopic factors and γ -decay widths are given in Tables II and III. These were used to obtain the proton-decay widths $\omega\gamma$ given in Tables II and III.

The top panel of Fig. 6 shows the total reaction rate versus temperature $T9$ (GK) for $^{34}\text{gCl}(p, \gamma)^{35}\text{Ar}$ from the 0^+ ground state of ^{34}Cl . The bottom panel shows the contribution from individual resonances given in Table II. The spectroscopic factors for the states in Table II are half of those in Table I for ^{34}S due the difference in the C^2 factor.

TABLE III. Properties of the resonance states for $^{34m}\text{Cl}(p, \gamma)^{35}\text{Ar}$ from 5.8 to 6.8 MeV. $J_i^\pi = 3^+$. $Q = 6.042$ MeV. n is the number of the level in the spectrum. k is the number of the level for a given J^π value. $\text{C}^2\text{S}^+ = [(2J_f + 1)/(2J_i + 1)] \text{C}^2\text{S}$.

n	J^π	k	$E_x(\text{th})$ (MeV)	E_{res} (MeV)	C^2S^+ $\ell = 0(1)$	Γ_γ (eV)	Γ_p (eV)	$\omega\gamma$ (eV)
31	$5/2^-$	3	5.823		4.8×10^{-3}	1.7×10^{-1}		
32	$5/2^+$	5	5.836		5.4×10^{-2}	5.6×10^{-2}		
33	$7/2^-$	4	5.871		5.3×10^{-2}	2.8×10^{-2}		
34	$9/2^-$	3	5.928		1.6×10^{-3}	1.9×10^{-3}		
37	$5/2^-$	4	6.048		3.8×10^{-3}	6.8×10^{-2}		
38	$7/2^-$	5	6.113	0.071	5.3×10^{-2}	4.6×10^{-2}	8.5×10^{-19}	4.9×10^{-19}
39	$3/2^-$	4	6.142	0.100	6.1×10^{-3}	4.9×10^{-2}	3.4×10^{-15}	9.7×10^{-16}
40	$9/2^-$	4	6.216	0.174	1.6×10^{-3}	6.8×10^{-3}	1.4×10^{-10}	9.7×10^{-11}
41	$5/2^-$	5	6.244	0.202	1.9×10^{-2}	8.9×10^{-2}	3.9×10^{-8}	1.7×10^{-8}
42	$3/2^-$	5	6.338	0.296	6.2×10^{-3}	2.8×10^{-1}	1.1×10^{-5}	3.2×10^{-6}
43	$7/2^+$	4	6.377	0.335	2.8×10^{-2}	6.3×10^{-2}	5.1×10^{-4}	2.9×10^{-4}
44	$5/2^-$	6	6.401	0.359	6.6×10^{-5}	5.4×10^{-2}	1.5×10^{-6}	6.6×10^{-7}
45	$5/2^+$	6	6.415	0.373	3.2×10^{-4}	8.1×10^{-1}	3.5×10^{-5}	1.5×10^{-5}
46	$7/2^-$	6	6.445	0.403	1.9×10^{-5}	4.8×10^{-2}	2.7×10^{-6}	1.5×10^{-6}
48	$7/2^-$	7	6.518	0.476	1.7×10^{-1}	4.3×10^{-2}	9.5×10^{-2}	1.7×10^{-2}
49	$3/2^-$	6	6.519	0.477	8.1×10^{-2}	2.1×10^{-1}	9.0×10^{-2}	1.8×10^{-2}
50	$7/2^-$	8	6.598	0.556	2.8×10^{-2}	7.7×10^{-2}	9.0×10^{-2}	2.4×10^{-2}
51	$5/2^-$	7	6.687	0.645	2.3×10^{-1}	3.7×10^{-1}	4.6	1.5×10^{-1}
55	$5/2^-$	8	6.749	0.707	2.6×10^{-2}	1.4×10^{-1}	1.3	5.4×10^{-2}
56	$9/2^-$	5	6.805	0.763	2.3×10^{-1}	1.7×10^{-2}	1.4×10^1	1.2×10^{-2}

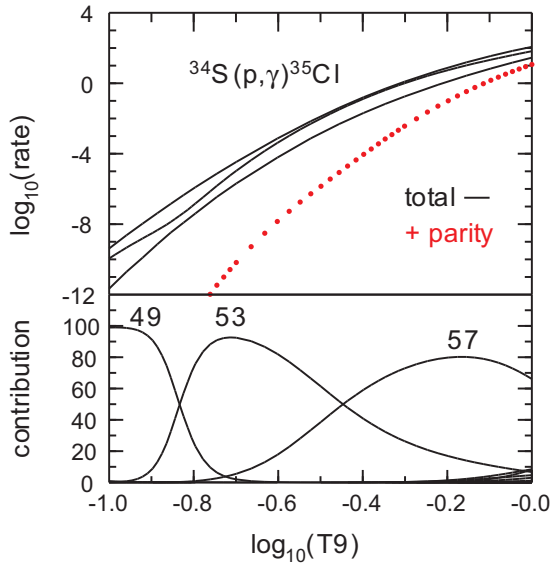


FIG. 4. Top panel: The calculated reaction rate for $^{34}\text{S}(p, \gamma)^{35}\text{Cl}$ vs temperature T_9 (GK). The upper and lower black lines show the low and high rates obtained from the Monte Carlo calculations. The middle black line shows the rate obtained directly from the input in Table I. The results from positive parity states only are shown by the red dots. Bottom panel: The contribution of individual resonances in Table I.

The top panel of Fig. 7 shows the total reaction rate versus temperature T_9 (GK) for $^{34m}\text{Cl}(p, \gamma)^{35}\text{Ar}$ from the 3^+ isomeric state of ^{34}Cl at 0.146 MeV. The bottom panel shows the contribution from individual resonances given in Table III. The rate is dominated by an $L = 0$ transition to a $7/2^+$ state.

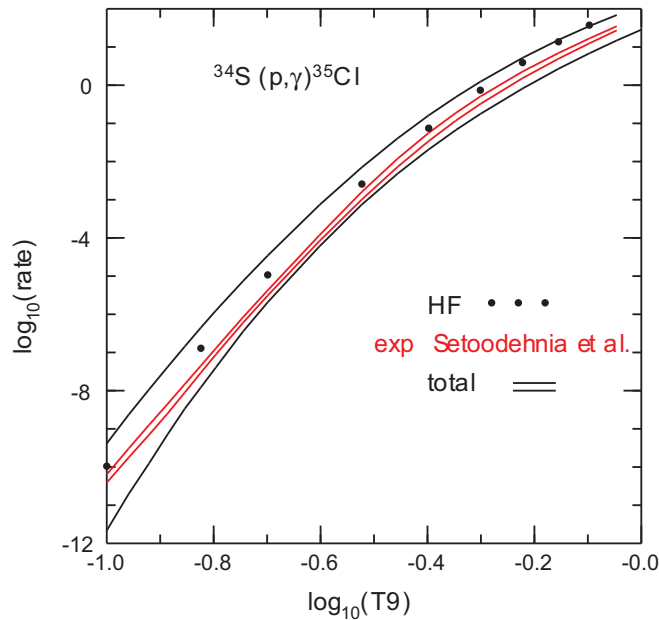


FIG. 5. The calculated reaction rates for $^{34}\text{S}(p, \gamma)^{35}\text{Cl}$ compared with the rate [8] based on experimental data from Ref. [7] and the Hauser-Feshbach rate from Ref. [21].

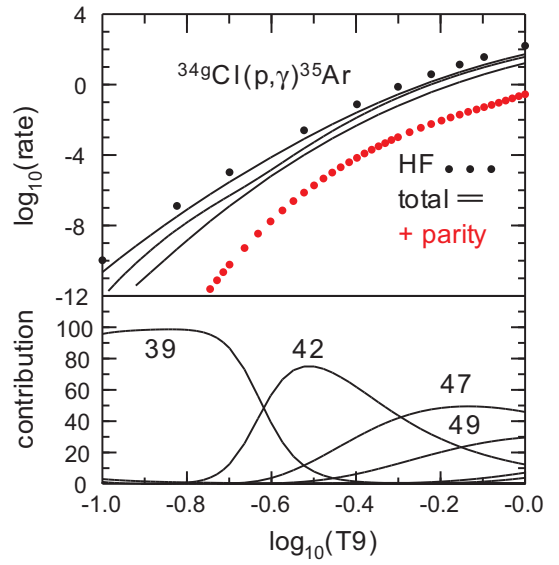


FIG. 6. Top panel: The calculated reaction rates for $^{34g}\text{Cl}(p, \gamma)^{35}\text{Ar}$ vs temperature T_9 (GK). The upper and lower black lines show the low and high rates obtained from the Monte Carlo calculations. The middle black line shows the rate obtained directly from the input in Table II. The results from positive-parity states only are shown by the red dots. The results are compared to the Hauser-Feshbach rate from Ref. [21]. Bottom panel: The contribution of individual resonances in Table II.

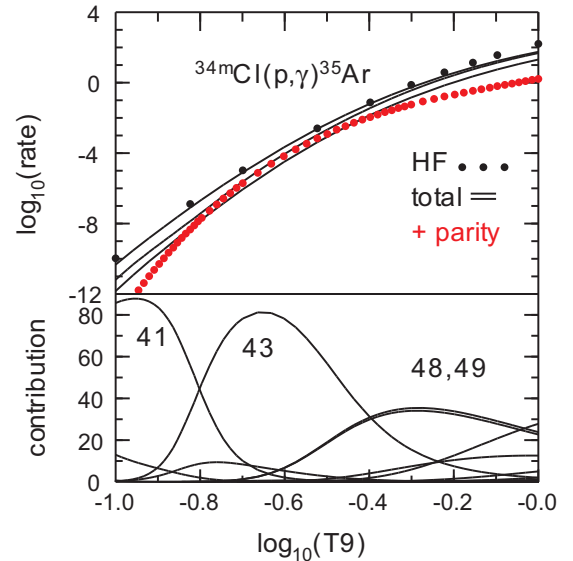


FIG. 7. Top panel: The calculated reaction rates for $^{34m}\text{Cl}(p, \gamma)^{35}\text{Ar}$ vs temperature T_9 (GK). The upper and lower black lines show the low and high rates obtained from the Monte Carlo calculations. The middle black line shows the rate obtained directly from the input in Table III. The results from positive-parity states only are shown by the red dots. The results are compared to the Hauser-Feshbach rate from Ref. [21]. Bottom panel: The contribution of individual resonances in Table III.

The increase in the reaction rate due to thermal population of an excited state is referred to as a stellar enhancement factor (SEF). In the case of ^{34}Cl , the reaction rate from the isomeric state is much larger than from the ground state, leading to a large SEF. The previous calculation reported for $^{34g,m}\text{Cl}$ [22] is only based on the sd -shell results for positive-parity states, resulting in rates that are much smaller than those obtained here with the inclusion of the negative-parity states.

IV. NUCLEOSYNTHESIS SIMULATIONS

The astrophysical implications of the present shell-model calculations were investigated using the Nova framework [23], which combines the stellar evolution code MESA with the postprocessing nucleosynthesis tools of NuGrid. An oxygen-neon (ONe) white dwarf of 1.3 solar masses and an initial luminosity of $\log_{10}(L/L_{\odot}) = -2.52$ was assumed along with a mass accretion rate of 2×10^{-10} solar masses per year, where the accreted material consisted of 50% solar and 50% ONe white-dwarf compositions [ONe denotes the elements O (oxygen) and Ne (neon)]. For the latter, we used the “Barcelona” ONe white-dwarf composition (see Fig. 4 in Ref. [23]). Using these parameters, the chemical composition of the nova ejecta is close to that of model ONe6 of Ref. [24] (see Fig. 11 in Ref. [23]). The maximum temperature of H burning in our model reaches 355 MK. The thermonuclear rates employed were initially identical to those used in Ref. [23], except we adopted the recently improved $^{33}\text{S}(p, \gamma)^{34}\text{Cl}$ reaction rate from Parikh *et al.* [25], and the $^{34}\text{S}(p, \gamma)^{35}\text{Cl}$, $^{34g}\text{Cl}(p, \gamma)^{35}\text{Ar}$, and $^{34m}\text{Cl}(p, \gamma)^{35}\text{Ar}$ reactions were adopted from the present work. Thermal communication between the ground and metastable states of ^{34}Cl through all low-lying ^{34}Cl states was implemented [5]. Using the median rates under these assumptions, we find the $^{34}\text{S}/^{32}\text{S}$ mass-fraction ratio for nova ejecta to be 0.049. When the $^{34g}\text{Cl}(p, \gamma)^{35}\text{Ar}$ and $^{34m}\text{Cl}(p, \gamma)^{35}\text{Ar}$ rates are varied together within their uncertainties, the ratio barely changes. When the $^{34}\text{S}(p, \gamma)^{35}\text{Cl}$ rate is varied within its uncertainties, the ratio varies from 0.044 to 0.057. Varying all three reaction rates together leads to the most extreme range of 0.043 to 0.057.

Evidently, the nuclear physics uncertainties calculated for the reactions considered in the present shell-model calculations have only a moderate impact on the uncertainties associated with this isotopic ratio. Despite the large uncertainties associated with the individual resonance energies, the density of states is high enough that the resonances tend to compensate for each other statistically. The resulting variations in the thermonuclear reaction rates are not large enough to cause dramatic variations in this isotopic ratio.

The sulfur ratios presented above are centered near the solar value of 0.047 and are indistinguishable from the range of isotopic ratios predicted from core collapse supernovae (CCSN) models. For instance, models from Refs. [7] and [26] estimated a $^{34}\text{S}/^{32}\text{S}$ ratio for CCSN models in the range of 0.026 and 0.053. However, the observed $^{34}\text{S}/^{32}\text{S}$ ratio from presolar SiC grains of types X and C condensed in CCSN ejecta range between 0.003 and 0.036. The lowest observed ratio is comparable to a basically pure ^{32}S composition that is not reached in any part of the CCSN ejecta according to stellar

simulations [27]. This discrepancy was solved by considering the contribution of ^{32}Si in C-rich He-shell ejecta: ^{32}Si has an half-life of 172 years and is condensing as Si in SiC grains, much more efficiently than S [28]. This will produce an anomalously low $^{34}\text{S}/^{32}\text{S}$ ratio in the presolar grain, mainly due to the Si/S fractionation. Fujiya *et al.* [29] analyzed the isotopic ratios of S in presolar SiC of type AB, which among many different stellar sources could also be made in CCSN ejecta [30]. In these types of grains, the range of measured $^{34}\text{S}/^{32}\text{S}$ is going between 0.027 and slightly higher than solar.

In summary, the $^{34}\text{S}/^{32}\text{S}$ ratio measured in presolar grains made in CCSN is extremely large once the ^{32}Si radiogenic contribution to ^{32}S and the Si/S fractionation are taken into account, covering also the typical values obtained from novae simulations.

This unfortunate conclusion is different from the conclusion of Ref. [7], where a distinct range of 0.014 to 0.017 was derived for the nova grains based on indirect measurements of the $^{34}\text{S}(p, \gamma)^{35}\text{Cl}$ reaction rate and the code SHIVA. A recent study by Setoodehnia *et al.* [8] suggests that the experimental $^{34}\text{S}(p, \gamma)^{35}\text{Cl}$ reaction-rate uncertainties reported in Ref. [7] may have been underestimated. However, the present $^{34}\text{S}(p, \gamma)^{35}\text{Cl}$ rates agree with those reported in Ref. [7] and therefore the discrepancy must lie elsewhere. We notice that when we repeated the network-calculation procedure above using older rates [21,31] for the $^{33}\text{S}(p, \gamma)^{34}\text{Cl}$ reaction, we found isotopic ratios in the range of 0.024 to 0.034, which are closer to those reported in Ref. [7]. Similarly, the $^{30}\text{P}(p, \gamma)^{31}\text{S}$ reaction rate can strongly influence the production of ^{34}S and other nuclides in novae [32] and is still essentially unknown experimentally despite a variety of dedicated efforts over the past 15 years [33]. It may be the case that different assumptions about the rates of these other reactions led to different resulting isotopic ratios. It is therefore important that all influential reaction rates are constrained.

V. CONCLUSIONS

In the comparison of our calculations for $^{34}\text{S}(p, \gamma)^{35}\text{Cl}$ with the recent experiments of Gillespie *et al.* and Setoodehnia *et al.* on $^{34}\text{S}(^3\text{He}, d)^{35}\text{Cl}$, there is generally good agreement between the calculated total rate and the experimental rate. Since ^{35}Ar is the mirror nucleus to ^{35}Cl , this gives us some confidence in the calculation of the $^{34g,m}\text{Cl}(p, \gamma)^{35}\text{Ar}$ rates.

The $^{34}\text{S}(p, \gamma)^{35}\text{Cl}$ and $^{34g,m}\text{Cl}(p, \gamma)^{35}\text{Ar}$ rates are all dominated by $L = 1$ transitions. The $L = 1$ are particularly strong for the $^{34m}\text{Cl}(p, \gamma)^{35}\text{Ar}$ reaction. The statistical Hauser-Feshbach rate differs from our total rate at lower temperatures but converges to our rate for higher temperatures. The calculations also identify the most prominent resonances in the reaction rates, and the analysis should serve as a guide for experiments as the spin-parity assignments of the most prominent resonances and their relative strengths are given.

The rates were implemented in a NOVA nucleosynthesis code including thermal population of the ^{34m}Cl isomer. Nucleosynthesis uncertainties associated with the shell-model calculations are not very large. We find that, in contrast to recent work, the $^{34}\text{S}/^{32}\text{S}$ isotopic ratio is not a strong discriminator of presolar grains of nova origin.

ACKNOWLEDGMENTS

This work is partly supported by NSF Grants No. PHY-1811855, No. PHY-1565546, and No. PHY-1913554; No. PHY-1430152 (JINA Center for the Evolution of the Elements); and DOE Grant No. DE-SC0016052. R.L. acknowledges support from US Department of Energy Grant No. DE-SC0017799 and Contract No. DE-FG02-97ER41041, and W.R. acknowledges support from the University of Stel-

lenbosch and iThemba LABS, South Africa. M.P. acknowledges significant support to NuGrid from STFC (through the University of Hull's Consolidated Grant No. ST/R000840/1), and access to VIPER, the University of Hull High Performance Computing Facility. M.P. acknowledges the support from the "Lendulet-2014" Program of the Hungarian Academy of Sciences (Hungary), and the ERC Consolidator Grant funding scheme (Project RADIOSTAR, Grant Agreement No. 724560, Hungary).

-
- [1] N. Liu, L. R. Nittler, C. M. O'D. Alexander, J. Wang, M. Pignatari, J. José, and A. Nguyen, *Astrophys. J.* **820**, 140 (2016).
 - [2] C. Fry, C. Wrede, S. Bishop, B. A. Brown, A. A. Chen, T. Faestermann, R. Hertenberger, A. Parikh, D. Pérez-Loureiro, H.-F. Wirth, A. García, and R. Ortiz, *Phys. Rev. C* **91**, 015803 (2015).
 - [3] A. Coc, M. G. Porquet, and F. Nowacki, *Phys. Rev. C* **61**, 015801 (1999).
 - [4] P. Banerjee, G. W. Misch, S. K. Ghorui, and Y. Sun, *Phys. Rev. C* **97**, 065807 (2018).
 - [5] R. Reifarh, S. Fiebiger, K. Goebel, T. Heftrich, T. Kauch, C. Koepfchen, D. Kurtulgil, C. Langer, B. Thomas, and M. Weigand, *Int. J. Mod. Phys. A* **33**, 1843011 (2018).
 - [6] H. Schatz, C. A. Bertulani, B. A. Brown, R. R. C. Clement, A. A. Sakharuk, and B. M. Sherrill, *Phys. Rev. C* **72**, 065804 (2005).
 - [7] S. A. Gillespie, A. Parikh, C. J. Barton, T. Faestermann, J. José, R. Hertenberger, H.-F. Wirth, N. de Séréville, J. E. Riley, and M. Williams, *Phys. Rev. C* **96**, 025801 (2017).
 - [8] K. Setoodehnia, J. H. Kelley, C. Marshall, F. Portillo Chaves, and R. Longland, *Phys. Rev. C* **99**, 055812 (2019).
 - [9] B. A. Brown and W. D. M. Rae, *Nucl. Data Sheets* **120**, 115 (2014).
 - [10] B. A. Brown, W. A. Richter, and C. Wrede, *Phys. Rev. C* **89**, 062801(R) (2014).
 - [11] R. Longland, C. Iliadis, A. E. Champagne, J. R. Newton, C. Ugalde, A. Coc, and R. Fitzgerald, *Nucl. Phys. A* **841**, 1 (2010).
 - [12] W. A. Richter and B. A. Brown, *J. Phys.: Conf. Series* **966**, 012026 (2018).
 - [13] B. A. Brown and W. A. Richter, *Phys. Rev. C* **74**, 034315 (2006).
 - [14] D. H. Gloeckner and R. D. Lawson, *Phys. Lett. B* **53**, 313 (1974).
 - [15] E. K. Warburton and B. A. Brown, *Phys. Rev. C* **46**, 923 (1992).
 - [16] B. A. Brown and B. H. Wildenthal, *Ann. Rev. Nucl. Part. Sci.* **38**, 29 (1988).
 - [17] E. K. Warburton, J. A. Becker, and B. A. Brown, *Phys. Rev. C* **41**, 1147 (1990).
 - [18] W. A. Richter, S. Mkhize, and B. A. Brown, *Phys. Rev. C* **78**, 064302 (2008).
 - [19] A. Graue, L. H. Herland, J. R. Lien, G. E. Sandvik, E. R. Cosman, and W. H. Moore, *Nucl. Phys. A* **136**, 577 (1969).
 - [20] W. A. Richter, B. A. Brown, A. Signoracci, and M. Wiescher, *Phys. Rev. C* **83**, 065803 (2011).
 - [21] C. Iliadis, J. M. D'Auria, S. Starfield, W. J. Thompson, and M. Wiescher, *Astrophys. J. Suppl.* **134**, 151 (2001).
 - [22] J. Grineviciute, B. A. Brown, and H. Schatz, *arXiv:1404.7268v1*.
 - [23] P. A. Denissenkov, J. W. Truran, M. Pignatari, R. Trappitsch, C. Ritter, F. Herwig, U. Battino, K. Setoodehnia, and B. Paxton, *Mon. Not. R. Astron. Soc.* **442**, 2058 (2014).
 - [24] J. José and M. Hernanz, *Astrophys. J.* **494**, 680 (1998).
 - [25] A. Parikh, K. Wimmer, T. Faestermann, R. Hertenberger, J. José, H.-F. Wirth, C. Hinke, R. Krücken, D. Seiler, K. Steiger, and K. Straub, *Phys. Lett. B* **737**, 314 (2014).
 - [26] A. Chieffi and M. Limongi, *Astrophys. J.* **764**, 21 (2013).
 - [27] P. Hoppe, P. Annen, R. Strebelt, P. Eberhardt, R. Gallino, M. Lugaro, S. Amari, and R. S. Lewis, *Astrophys. J. Lett.* **487**, L101 (1997).
 - [28] M. Pignatari *et al.*, *Astrophys. J. Lett.* **767**, L22 (2013).
 - [29] W. Fujiya, P. Hoppe, E. Zinner, M. Pignatari, and F. Herwig, *Astrophys. J. Lett.* **776**, L29 (2013).
 - [30] P. Hoppe, R. J. Stancliffe, M. Pignatari, and S. Amari, *Astrophys. J.* **887**, 8 (2019).
 - [31] A. L. Sallaska, C. Iliadis, A. E. Champagne, S. Goriely, S. Starrfield, and F. X. Timmes, *Astrophys. J., Suppl. Ser.* **207**, 18 (2013).
 - [32] C. Iliadis, A. Champagne, J. José, S. Starrfield, and P. Tupper, *Astrophys. J.* **142**, 105 (2002).
 - [33] C. Wrede, *AIP Adv.* **4**, 041004 (2014).